First-principles calculations to investigate structural, electronic and optical properties of BN by inserting an ultrathin XY(X = B, Al and Y= Bi, P, N) layer to form short-period (XY)1/(BN)1 superlattice

HAFIDA BELGHOUL[1], MIMOUNA OUKLI[1,*], FATIMA MOULAY[2], KARIMA GHLAM[1], HAMZA ABID[1]
[1]*Applied Materials Laboratory, Faculty of Electrical Engineering, Djillali Liabès University of Sidi Bel-Abbes, Algeria*
[2]*Department of Mechanical Engineering, Djillali Liabes University, BP 89 City Ben M'Hidi Sidi Bel-Abbès 22000, Algeria*

This study focuses on investigating the structural, electronic and optical properties of BN using first-principles analysis. To form a zinc-blende superlattice oriented following (001), (111), an ultrathin XY layer (where X = B, Al and Y = Bi, P, N) is inserted into the BN structure, using the full potential linear muffin-tin orbitals method (FPLMTO) within generalized gradient approximation (GGA96). Electronic structure analysis confirms that these compounds exhibit semiconductor behavior when oriented along the (001) axis with a direct (AlN)1/(BN)1 and indirect difference for the two other SLs. The analysis of the partial density of states reveals a significant influence of nitrided materials, such as BN, which can be attributed to the strong sp hybridization of N atoms. Furthermore, the dielectric functions, refractive index, and calculated absorption spectra of the (001) oriented superlattices demonstrate their potential for various technological applications in infrared and visible emission. We have found that our calculated values were in good agreement with those in the literature. In contrast, the (111) oriented systems exhibit semi metallic behavior. No experimental or theoretical studies have been conducted on the properties of (111)-oriented superlattices (SLs) composed of $(BBi)_1/(BN)_1$, $(BP)_1/(BN)_1$ and $(AlN)_1/(BN)_1$. So, this theoretical study provides valuable insight that can help in experimental measurements.

(Received February 19, 2024; accepted August 1, 2024)

Keywords: Superlattice, Growth axis, Boron bismuth, Boron nitride, Structural properties, Electronic structure, Optical properties

1. Introduction

In recent years, IIIV semiconductor compounds based on bore elements have played a great role in developing new technologies because of their use in electronic and optoelectronic applications, especially in the fabrication of solar cells, semiconductors, optical amplifiers, transistors, diodes, lasers, and other devices [1-3].

Particularly III-V semiconductor hetero-structures called superlattices (SL's) have attracted the particular necessity of searches for device applications and have come to be the subject of many theoretical and experimental investigations. The SL's focused attention due to the possibility of designing structures and the probability of adjusting band gaps and band structures with variations of simple parameters like superlattice period, growth direction, and substrate material [4-8].

It is evident that there has been a great deal of interest in the use of the first-principle calculations in materials science [10,11,12,14], including the density functional theory (DFT) [9,13] to study the structural and electronic properties of III–V semiconductors and their superlattice.

The physical properties of B-V compounds have been the subject of a great deal of theoretical research and experimentation. Ustundag et al. [3] have investigated the phase stability of B–V compounds in three different phases, namely Zinc-Blende (ZB), Rock-Salt (NaCl) and Wurtzite (WZ). They have found the ground state phase of B-Vcompounds as ZB alloys using the full potential linearized augmented plane wave (FP-LAPW) method in the framework of density functional theory (DFT) with the generalized gradient approximation (GGA) Shen et al. [15] have investigated the structural and electronic properties of wurtzite BAlNby using first principles calculations based on hybrid density functional theory and a projection scheme to identify band edges, Bencherif et al. [16] studiedthe structural and electronic properties of boron-based compounds BN, BP and BAs that have crystallized in the ZB phase and study the relative stability of the NaCl (rock salt) and CsC by using the method FP-LAPW their calculation of the electronic structure of BP and BAs indicates the presence of a fundamental indirect Merabet et al. [8] have calculated the structural, electronic and optical properties of bulk semiconductors BP and BAs in the zinc blend phase and their (BP)n/BA)n (n=1, 2 and 3) superlattices are performed using the. The fundamental band gap dependence of the SL on the number of SL monolayers is given. Arbouche et al. [17] have investigated the stabilities of four III-phosphide compounds: (BP, GaP, AlP, and InP) in zinc-blende. Ferhat and Zaoui [18] have investigated the properties of BBi in various phases using first principles calculations.

They have reported that the ZB phase is a more stable structure than the others for BBi.

In this paper we report first-principles investigations of structural, electronic and optical properties of BN by inserting an ultrathin XY(X = B, Al and Y= Bi, P, N) layer to form short-period $(YX)_1/(BN)_1$ superlattice oriented following the (001) and (111) by using the full potential linear muffin-tin orbitals method (FPLMTO) in its plane wave approximation (PLW), which enables an accurate treatment of the interstitial regions.

To date, though, the (BBi)m/(BN)n, (BP)m/(BN)n, and (AlN)m/(BN)n SL's with different growth axis directions have received little to no attention. Here, we aim to not only provide all the information regarding the (001) symmetries but also to investigate the symmetry of (111)-oriented SLs. Ultimately, we hope to be able to predict the precise structural, electronic and optical characteristics of SLs grown along the (001) and (111) direction using first principles calculations whose is devoid of adjustable parameters and can help shed light on different aspects of the problem.

The rest of the paper is organized as follows. We briefly describe the computational details used in the present work in Section 2, and the results about the structural, electronic, and optical properties are presented in Section 3 finally the work is concluded in Section 4.

2. Computational

The present study reports first-principles investigations of the structural and electronic properties of BN by inserting an ultrathin layers of XY (X = Al, Bi, P and Y= B, N) to from a short period superlattice $(XY)_1/(BN)_1$ oriented following the axes (001), (111) using the full potential linear muffin-tin orbitals method (FPLMTO) [19,20] as incorporated in the new version of the LMTART computer code within the generalized gradient approximation (GGA 96) [21,22,23,24] using the parameterization of Perdew et al. [25]. The FPLMTO method extends the potential of non-overlapping muffin-tin spheres (MTSs) to spherical harmonics within the sphere. In the interstitial region (IR), the basis functions s, p, and d are expanded into a set number (NPLW) of plane waves in the interstitial regions, effectively treating them equally as in the central regions. Automatic determination of cutoff energies establishes the value of (NPLW). The base set of LMTO and charge density are created using spherical harmonics up to lmax=6 (the highest possible angular momentum). We have verified the accuracy of the Fourier and mesh division parameters that play a role in these computations. Through an iterative process, the total energy is recalculated until it converges with a minimum accuracy of 10^{-4} Ry.

For binaries, a primitive cell is considered. Each position contains two atoms, the first being (B, Al) and the second being (Bi, P, or N). The second atom is obtained from the first atom by a shift of (1/4,1/4,1/4). a_0 in the zinc-blende (ZB) phase, a_0 being the lattice parameter of the binary Fig. 1-a among the structures being looked into are ideal quantum well superlattices SL (n, n) has a tetragonal symmetry made of a periodical sequence of m monolayers of BBI, BP or AIN atoms and n monolayers of BN atoms (n is the number of monolayers of binary compounds), (a monolayer contains two atoms, one cation, and one anion). We then select a series of (BBi)m/(BN)n, (BP)m/(BN)n, and (AlN)m/(BN)n, SL where $n = m$ =1 for all structural properties in the zinc mixture phase following the growth axes (001) Fig. 1-b and (111) Fig. 1-c.

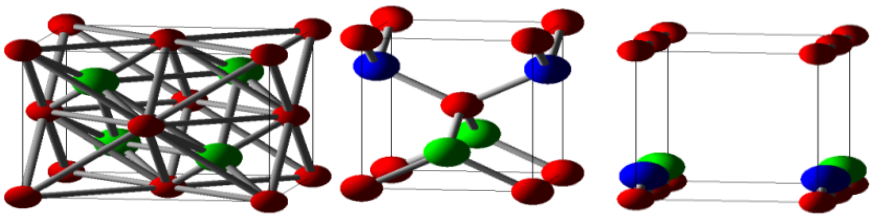

a b c

Fig. 1. Structure of the mesh of the zinc mixture of binaries and SL's oriented 001 and 111 (color online)

If we take (0 0 1) as the growth axis presented in Fig. 2, the x and y axes are parallel to the layer and the z axis that is perpendicular to it, and the primitive translational vectors of the superlattice (BBi)n/(BN)n, (BP)n/(BN)n and (AIN)n/(BN)n[SL's(n, n)] oriented (001) and are given by: $a_{x(001)}=\frac{a0}{2}$ (1 ,1 ,0); $a_{y(001)}=\frac{a0}{2}$ (-1 ,1 ,0); $a_{z(001)}=\frac{a0}{2}$ (0,0,L); Here the value of a_0 is a lattice constant of bulk materials, it should be noted that the period of our SLs is D=L*a_{SL}, a_{SL} being the equilibrium lattice constant of the SL's in the x direction ($a_{SL}=\frac{a0}{\sqrt{2}}$). The (001)- SL's unit cell has a tetragonal symmetry with $a_{x(001)}$= $a_{y(001)}$=a_{SL} =$\frac{a0}{\sqrt{2}}$ and $a_{z(001)}$ = L. a_0. The volume of the original direct unit cell (001) SL's is $V_{(001)} = L.a_0^3/2$ with 4L = 2(m + n).

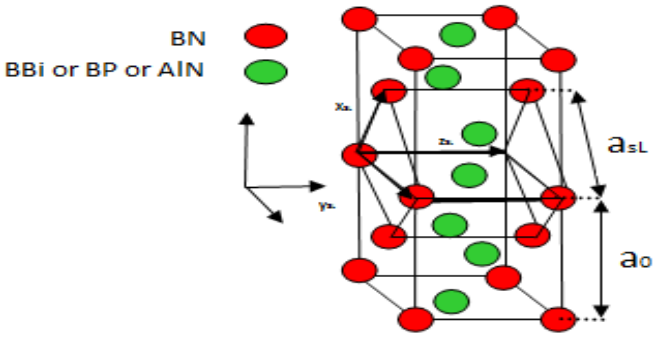

Fig. 2. The representation of the binary semiconductor and the superlattice of SL (1,1) along the growth axis (001). The set of primitive translation vectors of the superlattice is also shown as X_{SL}, YSL, and Z_{SL} for SL (1,1). i, j and k are the Cartesian unit vectors. Each point represents a node containing two atoms of the same species. a_0 and a_{SL} are the binary and superlattice network constants, respectively (color online)

The (111) oriented superlattices (SLs) presented in Fig. 3 are more intricate. The direct and reciprocal primitive cells of the (111) SLs are remarkably similar to those of the face centred cubic crystals (f.c.c) or the smallest ordered structure is a four-atom tetragonal cell corresponding to the SLs(1,1). The only difference is that one of the primitive translation vectors has a distinct length from the other two. Fig. 3 shows the unitary cell of the current SL(111), which is characterized by a non-orthogonal unitary basis set $(\overrightarrow{I_{SL}}, \overrightarrow{J_{SL}}, \overrightarrow{K_{SL}})$. $\overrightarrow{I_{SL}}$This unitary cell is slightly similar to the one corresponding to f.c.c. symmetry. However, there is a difference: the third vector has a different length, which is $\overrightarrow{K_{SL}}=\overrightarrow{L_i}+\overrightarrow{L_j}$for (111) SL's, while it is $\vec{K}=(\vec{\imath}+k)/2$ for f.c.c. To perform first-principle computations on (111) SL's, a different non-primitive cell was used, as shown in Fig. 2b. This cell is characterized by orthogonal vectors $(\overrightarrow{I_0}, \overrightarrow{J_0}, \overrightarrow{K_0}$. The volume of the current square tetragonal non-primitive cell is equal to 4 L a_0^3. It is easy to check that the multiplicity non-primitive cells is 8 by calculating the ratio V(111) non-primitive cells/V(111) primitive cells =8. Let us write down the lattice parameters of this tetragonal multiple unit cell. All are different: $a_{x(111)}$=a_{SL} = $\frac{a0}{\sqrt{2}}$, $a_{y(111)}$ = L.$\frac{a0}{\sqrt{2}}$, and $a_{z(111)}$ = 2. a_0. The points of high symmetry found in (111) SLs will bear a similarity to those in the f.c.c in two directions, but will diverge in the third direction by a consistent factor.

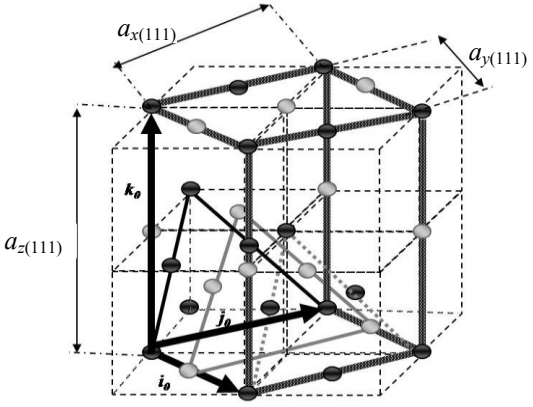

Fig. 3. Representing the link between the atomic planes of both the bulk semiconductor and the growth axis SL (111)

3. Results and discussion

3.1. Equilibrium structural properties

The objective of this work is to make a contribution in the field of design of optoelectronic devices based on III-V materials, this contribution is in the form of a study of the structural, electronis, and optical properties of SL's superlattices composed of two binaries for growth along the two axes (001) and (111). The choice fell on the four binaries BN, BBI, BP, and AIN. Relative to the binaries studied, a cubic unit cell of 8 atoms was considered. Each position contains two atoms, the first atom is that of boron (B) or aluminum (Al) located at position (0; 0; 0) a_0 and the second atom is that of nitrogen (N) the bismuth (Bi) or phosphorus (P), which is located at the position of (1/4; 1/4; 1/4) $a_0$in the zinc blend phase (a_0) which are the equilibrium lattice parameters of the two binaries).

The superlattice was first proposed by Esaki and Tsu in 1970 [26]. It is an artificial structure consisting of alternating layers of two different semiconductor materials, forming a periodic arrangement of quantum wells and barriers. In our case, each of these compounds (BBi) (BP), (AlN), acts as a barrier, while (BN) acts as a well. The study of structural and electronic properties in SL along the growth axes (001) has been considerably focused over the past decade, but the most interesting feature is knowing the effect of crystal orientations on their properties and potential applications [27] SL oriented (111) is reported to exhibit significantly different characteristics from those oriented along the (001) direction. The calculations in this work are carried out in ideal cases, where all the atoms of the binaries or SLs are located in ideal positions. By choosing SLs that have a short period, we can suppose that the lattice parameter is constant throughout the crystal, because the distance between successive interfaces is very small. This approximation frees us from any relaxation calculation. Atomic positions are among the most important factors for SL calculations.

We will present a detailed structural optimization by minimizing the total energy, the variations of the total energy as a function of volume for the binary compounds BBi, BP, AlN and BN, and the variation of the total energy

as a function of volume for SL (1,1) on the two growth axes (001) (111), respectively. From the adjustment of these curves by fitting using the Murnaghan equation [34], we calculated the mesh parameter (a_0), the bulk modulus B, and its derivative B'.

Tables 1 and 2 summarize the results of the calculations obtained by the FP-LMTO method with the GGA approximation; the iteration process is identical to that used for the calculation of binary and SL's systems, that is to say that all the energy converges with a minimum accuracy of 10^{-4} Ryd. The calculated results for the binary are presented in Table 1, which also contains results from early theoretical and experimental data for comparison. The calculated lattice parameters are in fairly good agreement with the experimental values [37, 39, 40, 41]. The calculated equilibrium lattice parameters of the binaries in ZB are 5.447 Å BBi, 4.554 Å BP, 4.3945 Å AlN and 3.617 Å BN underestimate the measured data by less than 0.35%, 0.32% and 0.05% from the experimental values of 4.538 Å for BP, 4.38 Å for AlN, and 3.615 Å for BN, respectively. Unfortunately, there is no experimental result for the binary compound BBi. However, note that for example, the lattice parameters for BBi were underestimated by 0.5 %compared to -5.479Å GGA [38], which ensures the reliability of the current calculations according to the first principles. This underestimate is attributed to our use of the generalized gradient approximation (GGA96), which is well known to slightly underestimate the lattice constant compared to the measured ones. We also found that our results for both compounds agree with those obtained by first-principles methods [1,3,8,16,32,33,35,36,37,30,39,40,41] in different approximations. We notice that the values obtained for the modulus of rigidity for our binary compounds are more or less close to the experimental results compared to other theoretical results. The calculated values of the compressibility modulus decrease as you go from BN to BBi, BN to BP, and BN to AlN according to Table 1, which verifies the relationship of inverse proportionality between the mesh parameter and the compressibility modulus.

Table 1. The structural parameters of the investigated compounds, V_0 is the equilibrium volume, a_0 represents the lattice constant of bulk materials. In the case of SL the link between a_0 and the SL lattice parameter is given by: ($a_0 = \sqrt{2}\ .a_{SL}$) for both (001) and (110) oriented SLs and ($a_0 = a_{SL} / \sqrt{2}$)for (111) oriented SLs. Bulk modulus B, pressure derivative B, compared to the available theoretical and experimental data

	V_0 (Å^3)	a_0 (Å)	a_{SL} (Å)	c_0/a_0	B	B'
BN	11.8389	3.61791	--	1	408.959	3.810
Exp		3.615 a			369 a 375.923b	4a 3 b
Theoretical studies		3.627b, 3.530c 3.63d			417.44 c 371.24 d	3.78 c 3.77 d
BBi	40.4028	5.447	--	1	74.289	4.311
Exp		5.479[29]			-------	-------
Theoretical studies		5.531b, 5.470 e 5.394f			66.846b 86.27g 83.99 f	4.395b 4.6 g 4.36 f
BP	23.6112	4.554	--	1		
Exp		4.538h			173i	------
Theoretical studies		4.551[3],4.425c 4.53j			161.734b 182.81c 153.19 j	3.649b 3.77 c 3.43 j
AlN	21.2162	4.3945	--	1	208.837	3.731
Exp		4.38k			-------- 201l	------ 3.66 l
Theoretical studies		4.377 l ,4.34m 4.349 n			209 m 211.78 n	3.38 m 3.90 n
(001) SLs						
BBi_1BN_1	28.4188	4.8393	3.422	1.414	57.5190	4 .35081
BP_1BN_1	18.1096	4.1686	3.3826	1.414	105.1819	3.3826
AlN_1BN_1	24.1156	4.437	4.5169	1.414	90.6615	4.5169
(111) SLs						
BBi_1BN_1	31.9812	4.7628	6.7356	1.414	166.5258	33.89898
BP_1BN_1	17.8605	4.452	11.17048	1.414	208.1572	11.17048
AlN_1BN_1	17.8748	4.476	9.9879	1.414	206.0380	9.9879

aRef [35], bRef [3], cRef [16], dRef [28], eRef [20], fRef [1], gRef [29], hRef [36], iRef [37], jRef[8], kRef [33], lRef [30], mRef [31], nRef [32]

To derive the fundamental characteristics of SL (1, 1), the total energies are calculated for six superlattice structures with varying volumes around the equilibrium volume V_0. The resulting values of total energy as a function of reduced volume are then reconciled using the Birch equation of state [39] to determine the properties of the ground state. Table 1 provides the equilibrium parameters (a_0, B and B') computed from the six superlattices. The lattice parameter of boron nitride is obviously smaller than that of boron bismuth, boron phosphide and aluminum nitride, as indicated by the ratio a_0 (BN)+a_0(BBi), a_0BN)a_0 (BP), and a_0(BN) a_0(AlN).

For BBi/ BN and BP/BN the cation atoms are identical in both compounds, and for AlN /BN the anion atoms are identical in both compounds, this result can easily be explained by considering the atomic radii of BI, P, Al and N, R (N) = 0.65 Å R(Bi)=1.60 Å, R(N)=0.65 Å R(P) =1.00 Å and R(N)= 0.65 Å R (Al) =1.25 Å. The lattice constant increases with increasing atomic size of anionic elements. We find $a_{1,1}$ oriented 001 and 111 equivalent to (a_0(BN)+a_0(BBi))/2, (a_0(BN)+a_0(BP))/2 and (a_0(BN)+ a_0 (AlN))/2 that the bulk modulus displays an increase in value as the orientation change from 001 to 111.

3.2. Electronic structure and density of states

Binary compounds BBi, BP, AlN, and BN and their superlattices. All calculations were carried out using the parameters of the equilibrium network theoretically optimized by the GGA96 approximation. The semiconductor behavior of the compounds is clearly shown in Fig. 4. This figure illustrate the calculated band structures of the compounds BN, BBi, BP, AlN, in which EF designates the Fermi level, the gaps relating to the parent binary compounds are compared with those obtained experimentally and theoretically in the zinc blend phase, the maximum of the valence band (VBmax) and the minimum of the conduction band (CBmin) are located at the point of symmetry x for the three binaries BN, BP and AIN which allows us to affirm that they belong to indirect gap semiconductors (Γ-Δ_{min}) and on the other hand the maximum of the valence band (VBmax) and the minimum of the conduction band (CBmin) are located at the point of symmetry Γ which allows us to affirm that they belong to direct gap semiconductors (Γ-Γ) for BBi. On examination of the results, it is evident that the existing estimated band gaps of 0.29 eV for BBi, 1.24 eV for BP, 3.41 for AlN and 4.90 for BN, for the most part lower than the corresponding experimental values of 1.24 eV for BP [27], 3.40 eV for AlN [35] and 4.85 eV for BN [40]. Unfortunately, there is no experimental result for the binary compound BBi. Note, however that, for example, the bandgap for theoretical studies of GGA [26] 0.26 eV of BB inerver the less, these estimates are consistent with other theoretical studies. The noticeable deviation between the calculated and experimental values of the band gaps can be attributed to the commonly known fact that, in DFT electronic band structure calculations, GGA tends to underestimate the energy gaps in semiconductors. However, these disparities will not affect the conclusions of this study, they do not relate to the precise assessment of the gaps.

Furthermore, the band structures and the variation of the gaps of SLs $(BBi)_1/(BN,)_1$, $(BP)_1/(BN)_1$ and $(AlN)_1/(BN)_1$ are calculated along the higher symmetry of the Brillouin zone (ZB) using the GGA96 approximation. (Figs. 5, 6) illustrate the calculated band structures of the SL's oriented (001) and (111) respectively. The objective of this study is to see the influence of symmetry parameters on these properties and more precisely the electronic properties. It should be noted that the higher symmetry points in the (111) SLs do not have the same meaning as in the binaries and the (001) SLs. From the results of the band gap energies of the SL calculated along the (001) axis, we note that these materials have an indirect band gap (Γ -M), the maximum valence band, and the minimum conduction band located at the point M, which is interesting for the design of infrared, except that for the $(AlN_1/(BN)_1$ which has a direct band gap (Γ-Γ), the maximum valence band and the minimum conduction band located at the point Γ, which is interesting for optoelectronic devices. The calculated SLs along the (001) axis, the results clearly show that the calculated band gap values are 0.26 eV for BBi/BN, 0.38 eV for BP/BN, and 2.01 eV for AlN/BN. We note that only the superlattice $(BP)_1/(BN)_1$ has preserved the nature of the indirect gap of its binary constituents BN and BP. To compare the gaps relating to superlattices with those obtained experimentally and theoretically, no results concerning the energy gaps of these superlattices are available in the literature.

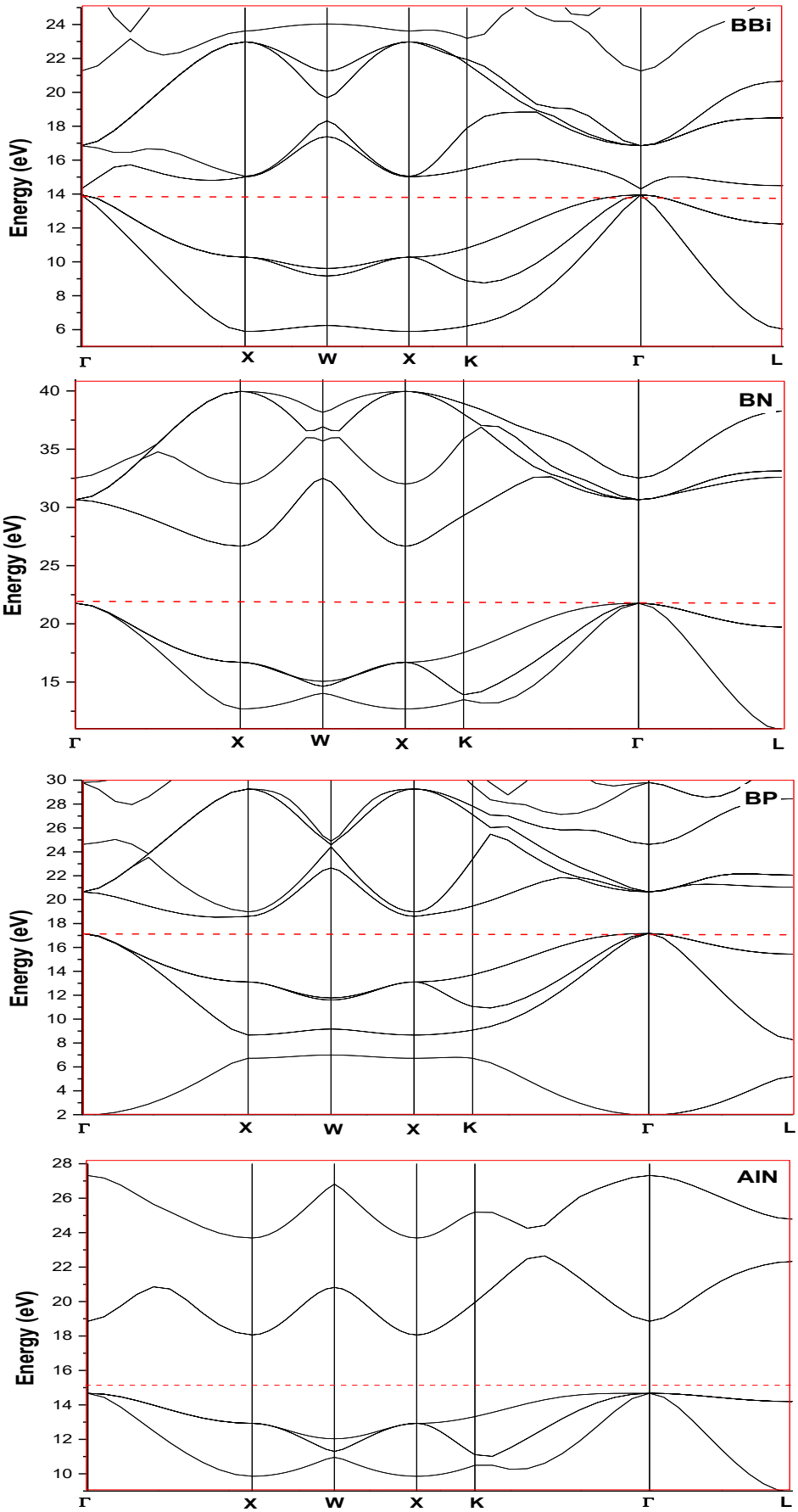

Fig. 4. The band structure of binary compounds (color online)

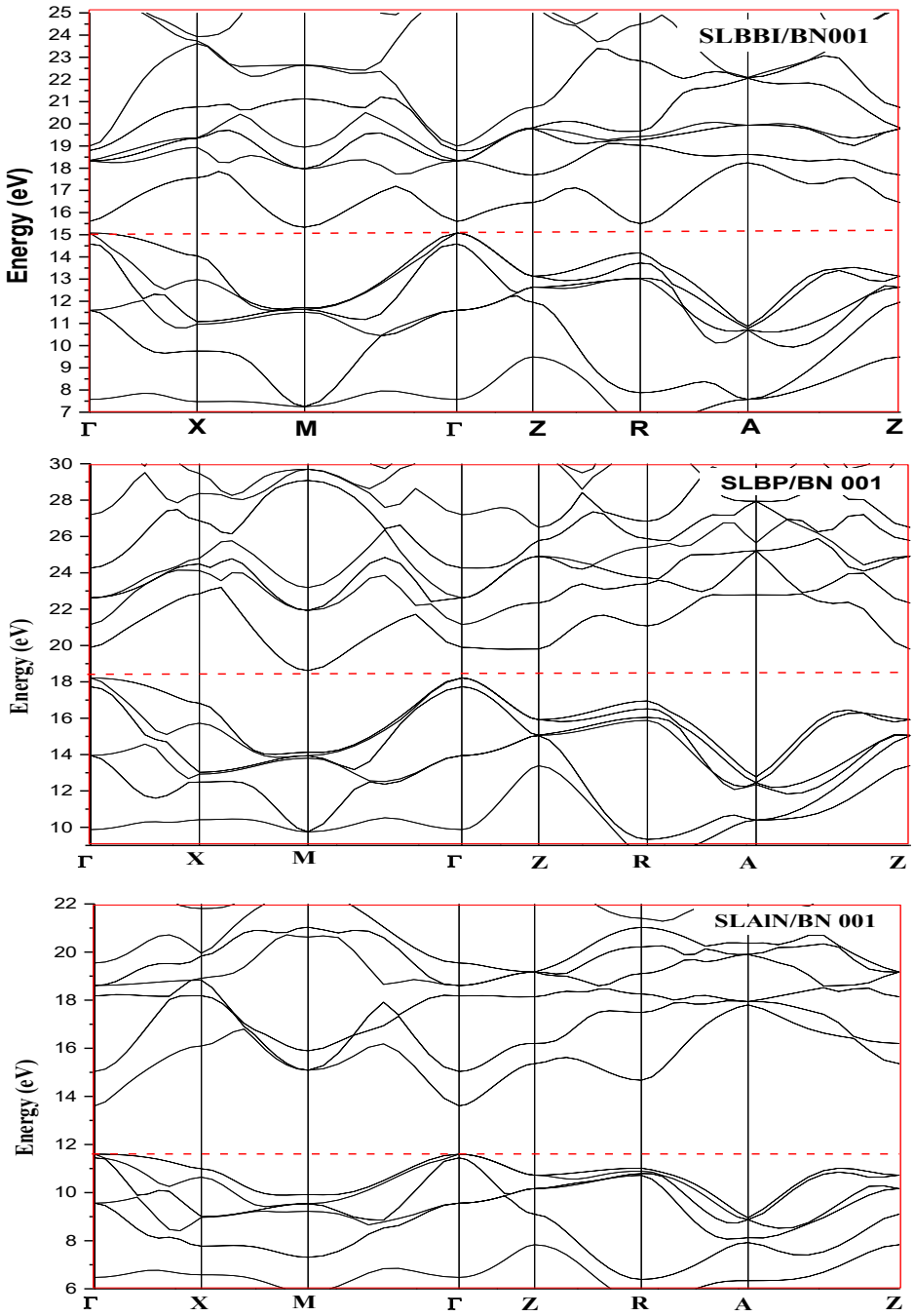

Fig. 5. The band structure of SL's (1,1) for (001) (color online)

The calculation of the band structure for the (111) orientation shows a large difference compared to the (001) orientation. The tetragonal Brillouin zone (BZ) of the SL (1,1) superlattice is (X, M, Γ, Z, R and A) in the case of direction (001) and those in the case of direction (111) are (X, M, Γ, Let B).The labels of the symmetry points used are calculated based on the following relationship:

$$\Gamma=(0,0,0) \tag{1}$$

$$M=\frac{2\pi}{aSL(111)}\left(-\sqrt{2}\underset{I_0}{\rightarrow}+\frac{\sqrt{2}}{2}\underset{K_0}{\rightarrow}\right) \tag{2}$$

$$L=\frac{2\pi}{aSL(111)}\left(-\frac{\sqrt{2}}{2L^2}\underset{J_0}{\rightarrow}+\frac{\sqrt{2}}{4L}\underset{K_0}{\rightarrow}\right) \tag{3}$$

$$X=\frac{2\pi}{aSL(111)}\left(\left(-\sqrt{2}\underset{I_0}{\rightarrow}-\frac{\sqrt{2}}{2L^2}\underset{J_0}{\rightarrow}\right)+\left(-\frac{\sqrt{2}}{2}+\frac{\sqrt{2}}{4L}\underset{K_0}{\rightarrow}\right)\right) \tag{4}$$

$$Z=\frac{2\pi}{aSL(111)}\left(-\sqrt{2}\right)\underset{K_0}{\rightarrow} \tag{5}$$

The electronic properties of crystalline materials depend on the symmetry of their crystal lattice. The (111) crystal orientation is generally associated with greater symmetry compared to the (001) orientation. Greater

symmetry can have an effect on the bandgap by influencing how atomic orbitals interact and overlap in the material. In our case, the greater symmetry led to a very small bandgap because the interactions between the electrons in the material are different from those in a less symmetric orientation. This can make electronic energy levels more favorable, reducing the bandgap width. The calculated SL along the (111) axis The results clearly show that the calculated band gap values are ~ 0ev therefore these materials have a zero band gap, which allows us to affirm that they belong to semi-metal. There is currently a lack of literature that provides any results on the energy gaps of superlattices, making it impossible to compare the experimental and theoretical data to the gaps of these particular structures.

The SLs structure, in the ideal configuration where all the atoms are located in the ZB sites, is obtained from the crystal. This helps to explain these changes in the band structure. One can assume that the SLs in this configuration come from the alternating superposition of trigonal layers of BBi and BN; of Bp and BN and AlN and BN. Consequently, the alterations and occurrences in the band structure SL can be comprehended through an examination of the atoms' orbitals and distinct chemical surroundings, resulting in a distinctive asymmetry in the valence charge density's electronic distribution and the bond charge surrounding these atoms. Thus, by directly comparing the various density of states (DOS) curves, it will be possible to have a clearer understanding of what is happening in the SL (001) and (111).

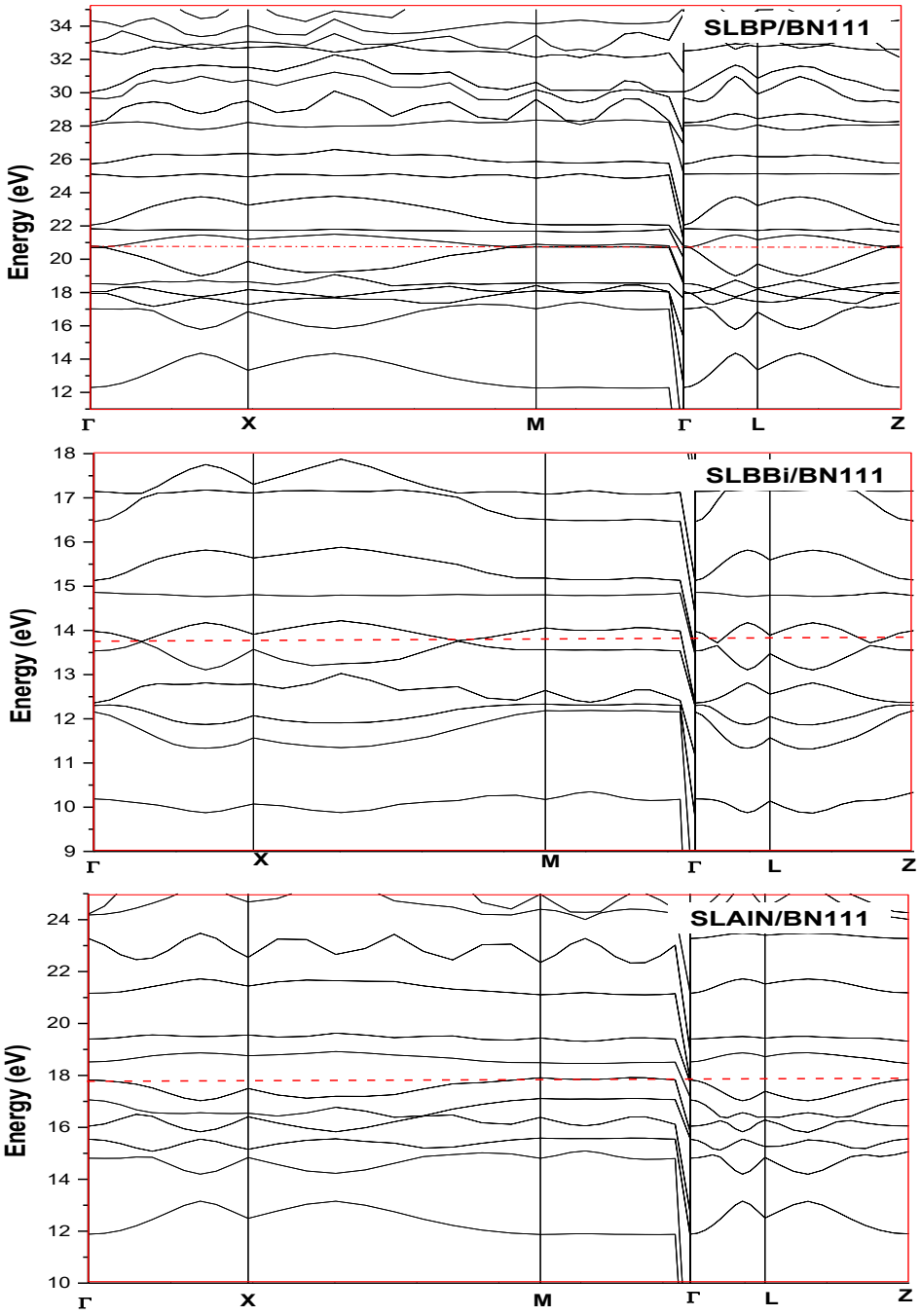

Fig. 6. The band structure of SL(1,1) for (111)

Calculating the density of states (DOS) is a crucial component in the examination of the electronic properties present in materials. When the occupancy rate of each atomic state is assessed, DOS also provides insight into the nature of chemical bonds within a material. Fig. 7 illustrates the total and partial densities of the equilibrium for the binary compounds BBi, BP, AlN, and BN in the zinc blend phase. By breaking down the total density and analyzing the contribution of each atomic character in a series of bands, we can gain a better understanding of the electronic structure of our compounds. To effectively analyze the density of states of superlattices, it is advantageous to first observe the behavior of the underlying binary components.

By examining the binary states, we can gain an initial understanding of their impact on SL. In Fig. 7, we illustrate the whole and partial density of the states of BN, BBi, BP, and AlN, we found that VB is close to the Fermi level Ef, in this region we notice the hybridization of the p orbital of (B) and the p orbital of (Bi) with the participation of s from (Bi) for the BBi, a domination of the p orbital of (P) with the participation of the p orbital of (B) for the BP, and for binary AlN we notice a domination of the p orbital of (N) with participation of the s and p orbitals of Al, the binary BN the p orbital of (N) is dominant.

The CB conduction band is formed by the hybridization of p from (B) and p from (Bi) with the participation of p from (Bi) with the participation of s from (B) and s from (Bi) for BBi binary, the hybridization of p from (B) and p from (P) and d from p of the BP compound, and for the AlN compound we notice the domination of p from (N)and the hybridization of s and p from (N) for BN.

On observation, it can be ascertained that boron-based materials such as BBi and BP compound are not substantially affected by boron orbitals. Conversely, materials that have been nitrided, such as AlN and BN, are highly susceptible to the influence of nitrides, such as the p orbital of N.

In the following we want to understand what happens in both cases of SL's by directly comparing the curves of the different density of states (DOS) and by analyzing the partial densities along the two growth axes in SL's. In Figs. 8, 9 and 10, we illustrate the complete and partial density of the states of SL $(BBi)_1/(BN)_1$, $(BP)_1/(BN)_1$ and $(AlN)_1/(BN)_1$ along the two growth axes. To demonstrate the contribution of orbitals from diverse areas, the bande of valence BV was categorized into subbands of low BV1, intermediate BV2, and high energy BV3. When considering oriented $(BBi)_1/(BN)_1$ (001) and (111), it is observable that the first zone BV1 (-7 eV to -5.3 eV) shows a contribution from the orbitals of (N) and s of (B2) for orientation (001), while the orbital s of (B2) dominates for orientation (111). Moving into the second zone BV2 (-5.3 eV to -2.6 eV), the orbital p of (N) is dominant with the involvement of the orbitals p of (Bi) and p of (B2) for orientation (001).

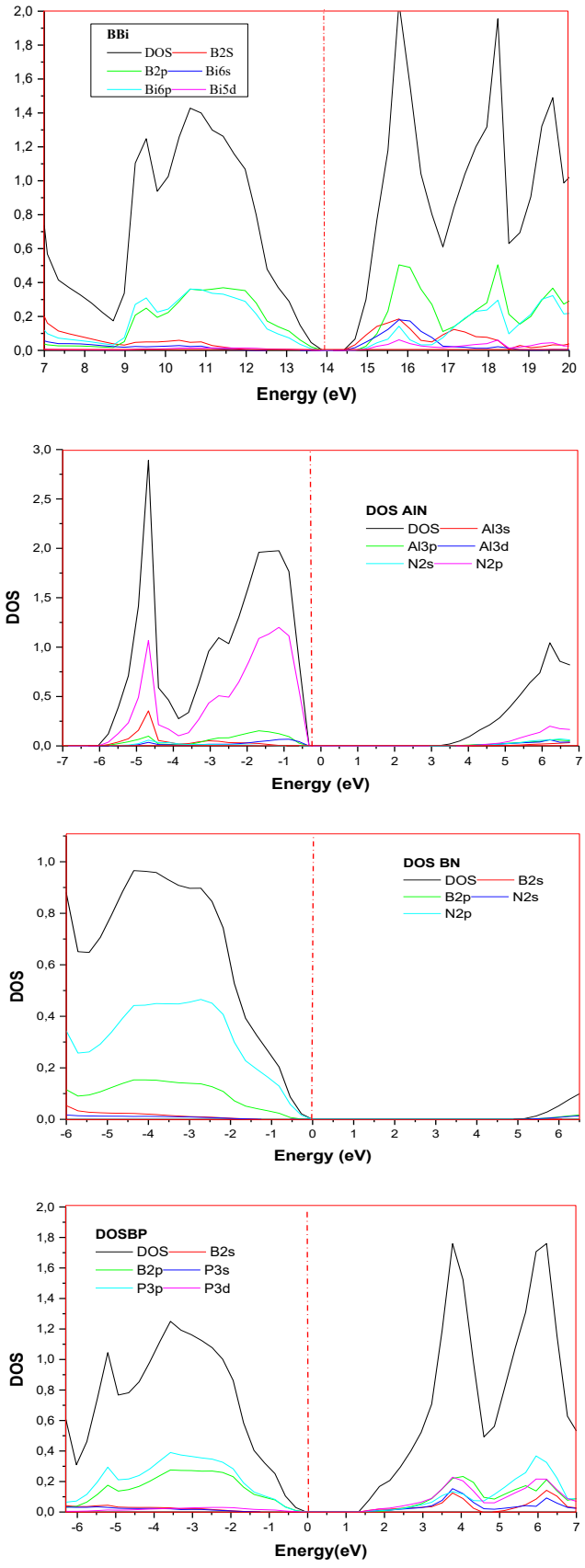

Fig. 7. The total and partial density of state (DOS) of binary compounds (color online)

For the (111) orientation, two pseudo-gaps are present, with the first being approximately 1.4 eV and the second approximately 0.8 eV. Between the two, the orbital of (B2) dominates with the participation of p of (N). In the third zone BV3 (-2.6 eV to 0 eV), the orbital p of (N) is dominant with the involvement of p of (B2) and p of (Bi) for orientation (001). Likewise, the orbital of (N) is dominant with the participation of the orbitals p of (B2) and p of (Bi) for the orientation (111). The presence of the s state of (B), p of (Bi), p from (B2), and p from (N) causes an overlap between the valence and conduction bands at the Fermi level. In the case of orientation (001), the CB conduction band is created through the hybridization of p from (N) and p from (B2), while that for orientation (111) is produced through the hybridization of p from (N) and p from (B2), with a slight involvement of p from (Bi). The results presented in this study demonstrate an unequivocal correlation between the dominant orbitals of the nitride atom, specifically p orbitals, and the upper valence band and lower conduction band in both the (001) and (111) superlattice orientations.

When considering the orientations $(BP)_1/(BN)_1$ oriented (001) and (111), the first zone BV1 (-7 eV to -5 eV) is characterized by the predominance of the p orbitals of (N) with the involvement of the p orbitals of (B2) and (P) for the orientation (001). For the orientation (111), the orbital of (P) dominates, resulting in a pseudogap of approximately 1.3 eV. In the second zone BV2 (-5 eV to -2 eV), the p orbital of (N) dominates with the participation of the (B2) and (P) p orbitals for the orientation (001). For the orientation (111), the p orbital of (N) prevails, partnering with the (P) p orbitals. In the third zone BV3 (-2 eV to 0 eV), the p orbitals of (N) dominate with the involvement of (B2) and (P)'s p orbitals for the orientation (001). Meanwhile, the orbital of (N) dominates for the orientation (111), resulting in an overlap between the valence and conduction bands at the Fermi level due to the presence of the p states from (N), p from (P), and p from (B2).

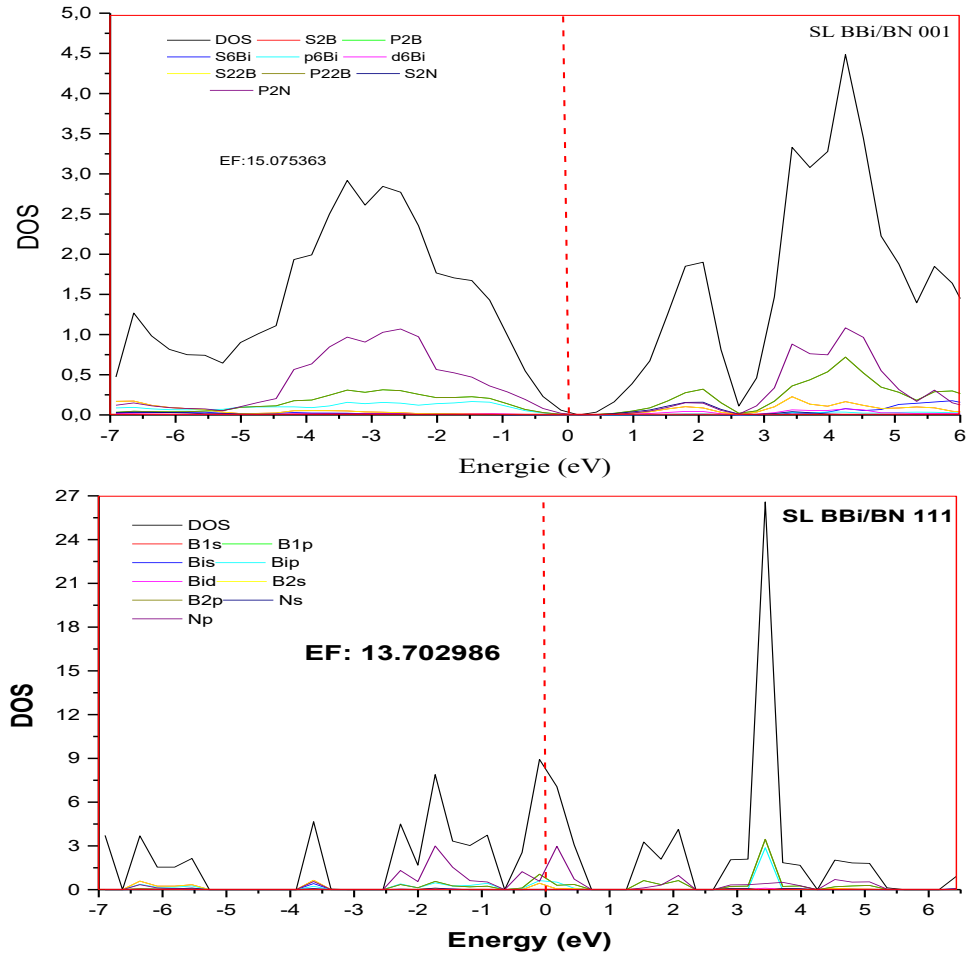

Fig. 8. The total and partial density of state (DOS) of SL $(BBi)_1/(BN)_1$ oriented (001) and (111) (color online)

The formation of the CB conduction band for orientation 001 is the result of the hybridization of (B2) and p from N with the participation of d from P. On the other hand, the formation of the 111 band occurs because the p orbitals of (N) dominate with the involvement of the p orbitals of (B2) and (P). The results indicate that the principal p orbitals of the nitride atom are congruent with the upper valence band and the lower conduction band in the SL orientation (001) and (111).

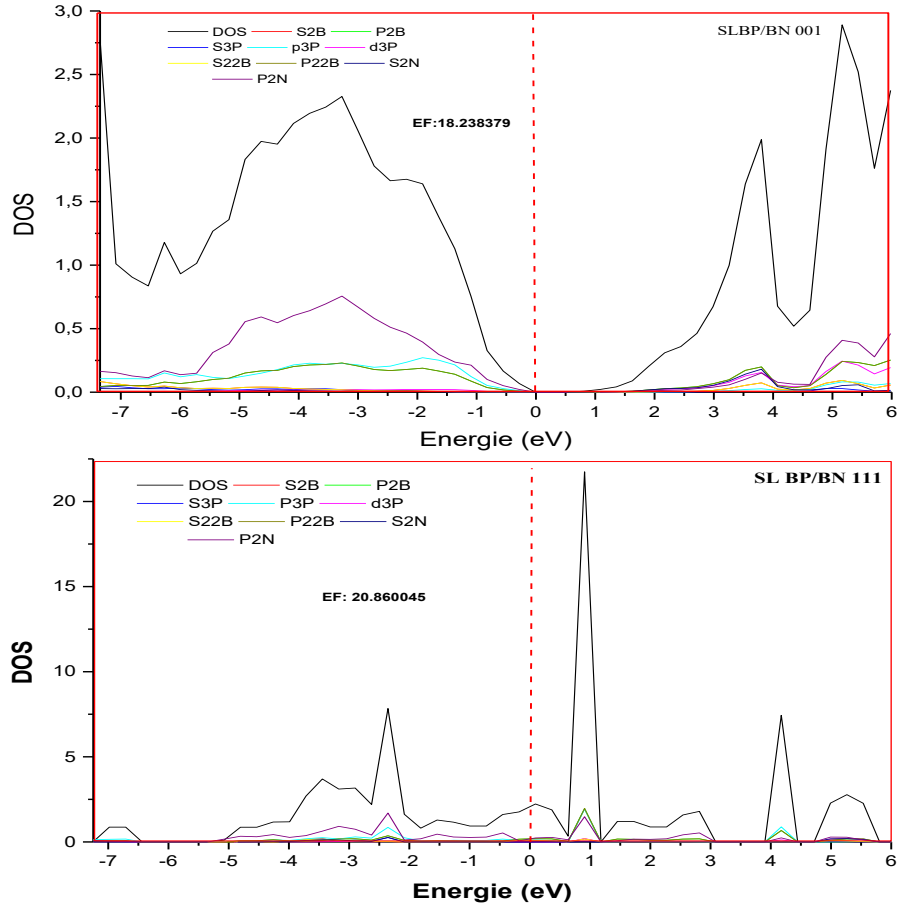

Fig. 9. The total and partial density of state (DOS) of SL $(BP)_1/(BN)_1$ oriented (001) and (111) (color online)

When considering the orientation $(AlN)_1/(BN)_1$ for both (001) and (111), the first zone BV1 (-6 eV to -4.4 eV) is characterized by the prevalence of the orbitals s of (B), with the help of the orbitals s of (N2) for orientation (001). However, for the orientation (111), the s orbitals of (B) dominate with the participation of the p orbitals of (N2). In the second zone BV2 (-4.4 to -2 eV), the orientation (001) is marked by the dominance of the s orbitals of (N2) with the involvement of the p orbitals of (B) and the s orbitals of (Al). In contrast, orientation (111) is characterized by the p orbitals of (N2) with the contribution of the p orbitals of (B), with the presence of pseudo-gaps of approximately 0.8 eV. Finally, in the third zone BV3 (-2 eV to 0 eV), the orientation (001) shows the domination of the s orbitals of (N2) with the participation of the p orbitals of (B), while the (111) orientation is dominated by the p orbitals of (N2) with the participation of the p orbitals of (B) The presence of the p state from (N2) causes an overlap between the valence and conduction bands at the Fermi level. The formation of the CB or conduction band for orientation 001 is a result of the amalgamation of p orbitals from (B) and s orbitals from (B). This is accomplished through the engagement of orbitals from (N2). On the contrary, the formation of 111 is achieved by hybridizing the p orbitals of (N2) and p orbitals of (B) with the collaboration of the p orbitals of (Al). The results of the study make it clear that the primary s and p orbitals of the nitride atom correspond to the higher valence band and lower conduction band in both the (001) and (111) superlattice orientations.

In this work, we investigate the optical properties of the bulk BBi, BP, AlN, and BN and their SLs $(BBi)_1/(BN)_1$, $(BP)_1/(BN)_1$and $(AlN)_1/(BN)_1$ oriented after (001) and (111). These essential properties of a material depend on the complex dielectric function ε (ω), the dielectric function, a useful tool for optical spectroscopy, can be computed from the electronic band structure computations of any material. Because it depends on frequency, the dielectric function of the electron gas has a big impact on the physical characteristics of materials. Keep in mind that the dielectric function describes the collective excitations of the Fermi sea, also known as the surface plasmons and volume.

The complex dielectric function versus frequency is a characteristic that characterizes the linear response of any material to an external electromagnetic field. It is generally possible to distinguish between the contributions of intra-band and inter-band electronic excitations to the complex dielectric function.

$$\varepsilon(\omega) = \varepsilon_1(\omega) + i\varepsilon_2(\omega) \quad (6)$$

where $\varepsilon_1(\omega)$ and $\varepsilon_2(\omega)$ are the real and imaginary parts of the dielectric function respectively [41]. To determine the imaginary component of the dielectric function in long wavelengths, an electronic structure calculation is conducted that involves examining the joint density of states and momentum matrix elements between occupied and unoccupied wave functions. From the imaginary parts, one can obtain the real part by the Kramers-Kronig relationship [42-46].

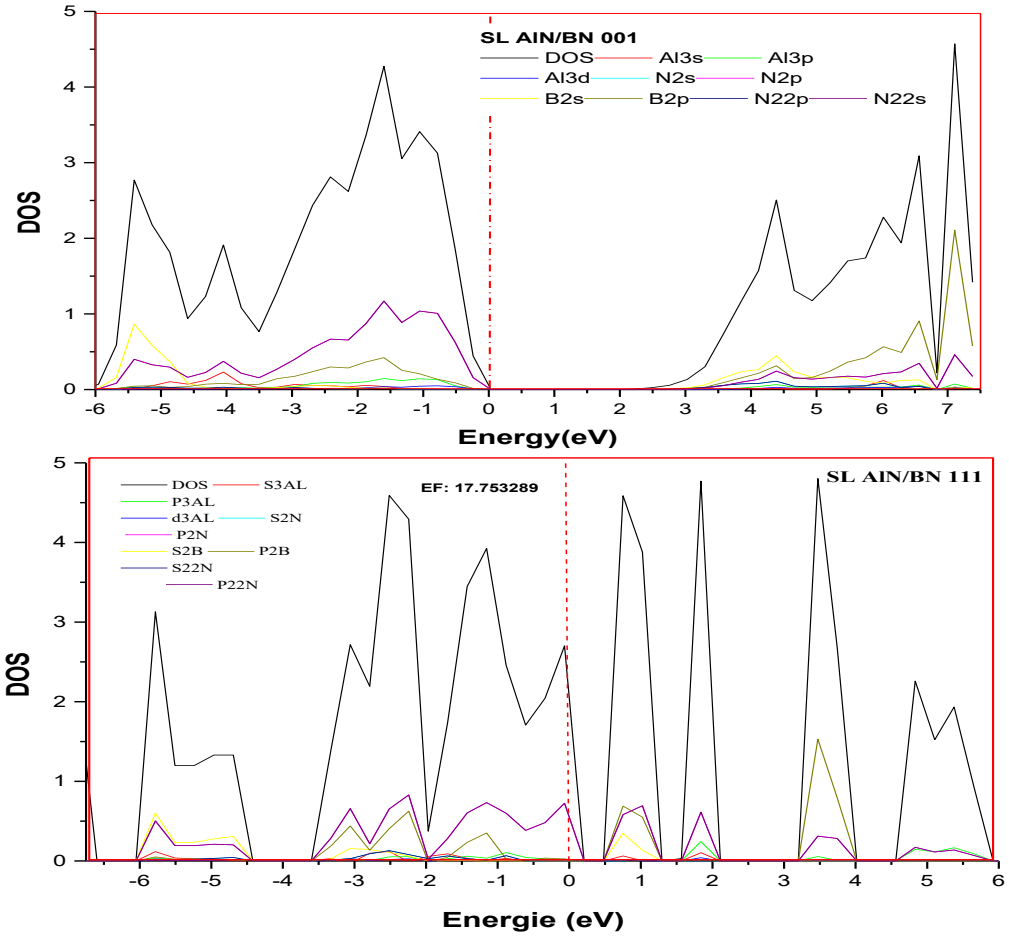

Fig. 10. The total and partial density of state (DOS) of SL $(AlN)_1/(BN)_1$ oriented (001) and (111) (color online)

The important optical constants can be derived from the real and imaginary parts of the dielectric function. In this paper we provide a presentation and a detailed analysis of the important optical function such as the refractive index n(ω) and the absorption coefficient a(E) [47,48], given by respectively:

$$n(\omega)=\left[\frac{\varepsilon_1(\omega)}{2}+\frac{\sqrt{\varepsilon_1^2(\omega)+\varepsilon_2^2(\omega)}}{2}\right]^{1/2} \quad (7)$$

$$\alpha(\omega)=\frac{4\pi}{\lambda}k(\omega) \quad (8)$$

where k is the extinction coefficient and is the wavelength of light in vacuum. A detailed description of the calculation of optical properties can be found in Ambrosch Draxland Sofo [49,50,51,52]. To compute the optical spectra of the dielectric function e(ω), a dense grid of uniformly distributed k points must be utilized. Therefore, the integration of the Brillouin zone was executed with 600 k points in the irreducible segment of the Brillouin zone for binary BBi, BP, AlN, and BN as well as their superlattices, without broadening, covering a range of up to 30 eV in energy.

The calculated real and imaginary parts of the dielectric function for bulk BBi, BP, AlN, and BN for both growth axes at zero pressure for radiation up to 30 eV are shown in Fig. 11.

The imaginary components of the dielectric function for four compounds are shown in Fig. 11. BBi, BP, AlN, and BN. It is important to note that the optical spectra represented in this figure differ from each other. When analyzing the $\varepsilon_2(\omega)$ spectra, certain critical points of the dielectric function are revealed. These points correspond to the fundamental absorption thresholds, which begin at around 0, 3.6, 4.5, 9.1 for BBi, BN, BP, and AlN, respectively. The optical transition between the top of the valence band and the bottom of the conduction band is responsible for the origin of these points. Specifically, for BBi, the transition occurs at Γ→ Γ, while for BP, AlN, and BN, it occurs at Γ→M. Upon close observation, it becomes apparent that the form of these spectrums demonstrates a rough approximation. There exists a

single significant peak E. The absorption thresholds coincide with the optical gaps. In the case of the four binary compounds, the highest point of absorption can be found at 4.7, 6.3, 7.9, and 12.8 eV for BBi, BN, BP, and AlN, respectively. The majority of optical transitions that result in peaks occur when the occupied orbital of B, Bi, P, Al, and N atoms situated at the peak of the valence band shifts to the empty orbital of the atoms located at the bottom of the valence band, the conduction band. The real variation of the variation of the dielectric function part variation $\varepsilon_1(\omega)$ is depicted in Fig. 11 as a function of energy. The spectra show high intensity peaks at 1.2, 4.8, 6, and 12 eV for BBi, BN, BP, and AlN, respectively, which is commonly known as the fundamental absorption threshold. Additionally, it should be noted that $\varepsilon_1(\omega)$ becomes negative at approximately 4, 6.5, 11.8, 13 eV for BBi, BN, BP and AlN, respectively. Referring to the calculated values in Table 2, which represent the static value of $\varepsilon_1(\omega)$ corresponding to a zero frequency or $\varepsilon(0)$, we observe that materials with a low energy gap exhibit a significant value of dielectric function This phenomenon is explained by the Penn model [53,54], which is expressed as:

$$\varepsilon_1(0) \approx 1 + \left(\frac{\hbar\omega_p}{E_g}\right)^2 \tag{9}$$

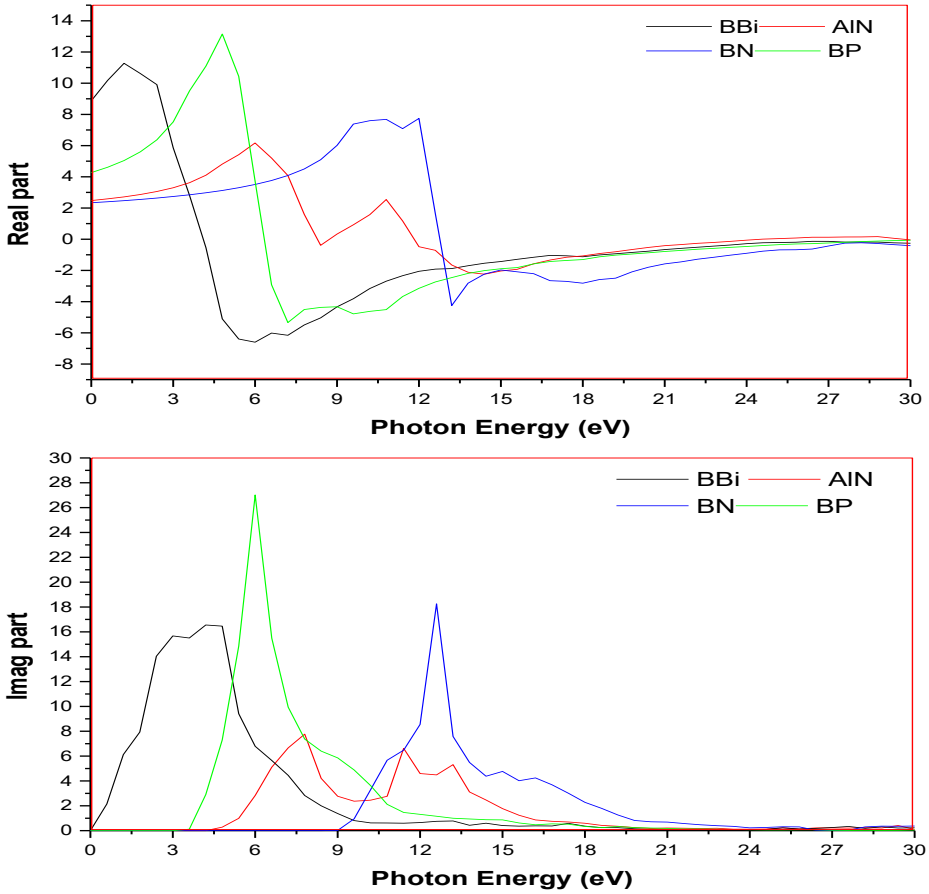

Fig. 11. Calculated dielectric functions (real and imaginary parts) for binary compounds (color online)

The study of refractive indices in binary compounds was carried out using expression (7). Fig. 12 shows the results obtained from our research. Static refractive indices, n(0), of the binaries were estimated through the refraction spectra (Table 2). BBi exhibited significantly higher values of n(0) and ε1(0) in comparison to the other binaries due to the high atomic number of bismuth. The maximum refractive index was achieved for the photon energy around 2.8 eV for BBi, 6 eV for BP, 6.1 eV for AlN, and 13 eV for BN. The absorption spectra of the binaries are shown in Fig. 12. The absorption threshold was observed to begin at energy levels of 0.5 eV, 3.8 eV, 4.5 eV and 9 eV for BBi, BP, AlN and BN, respectively. The evolution of these spectra demonstrated that the values of $\alpha(\omega)$ reached their maximum levels at energies of approximately 8.8 eV, 10.7 eV, 13 eV and 12.8 eV for BBi, BN, BP and AlN, respectively, after which the absorption coefficient decreased for energies above 30 eV.

Table 2. Calculated static optical constants $\varepsilon_1(0)$ and static refractive index n(0) for binary compounds

Compounds	$\varepsilon_1(0)$	n(0)
BBi	8.8702	2.97829
BP	4.2694	2.06625
AIN	2.477	1.5741
BN	2.33636	1.5285

To represent all possible optical transitions in SL $(BBi)_1/(BN)_1$, $(BP)_1/(BN)_1$and $(AlN)_1/(BN)_1$ along the two growth axes, we added the special. The number of points in the first ZB is up to 600 k points, and the energy range is up to 30 eV. Figs. 13, 14, 15 show the real and imaginary parts of the connected dielectric function for $(BBi)_1/(BN)_1$, $(BP)_1/(BN)_1$, and $(AlN)_1/(BN)_1$ in two growth axes compared to their binary compounds. The appearance of peaks in $\varepsilon_2(\omega)$ is mainly caused by optical transitions between the band or the intraband. In both cases (001) and (111), the $\varepsilon_2(\omega)$ spectrum appears as an optical transition between the filled and empty states of different SLs, the 111 oriented SLs are very different and reflect different optical transitions, with the peaks moving towards more. The high –energy shift, which can be attributed to the larger electronegativity of N, strongly depends on the ionic polarization of the SLs.

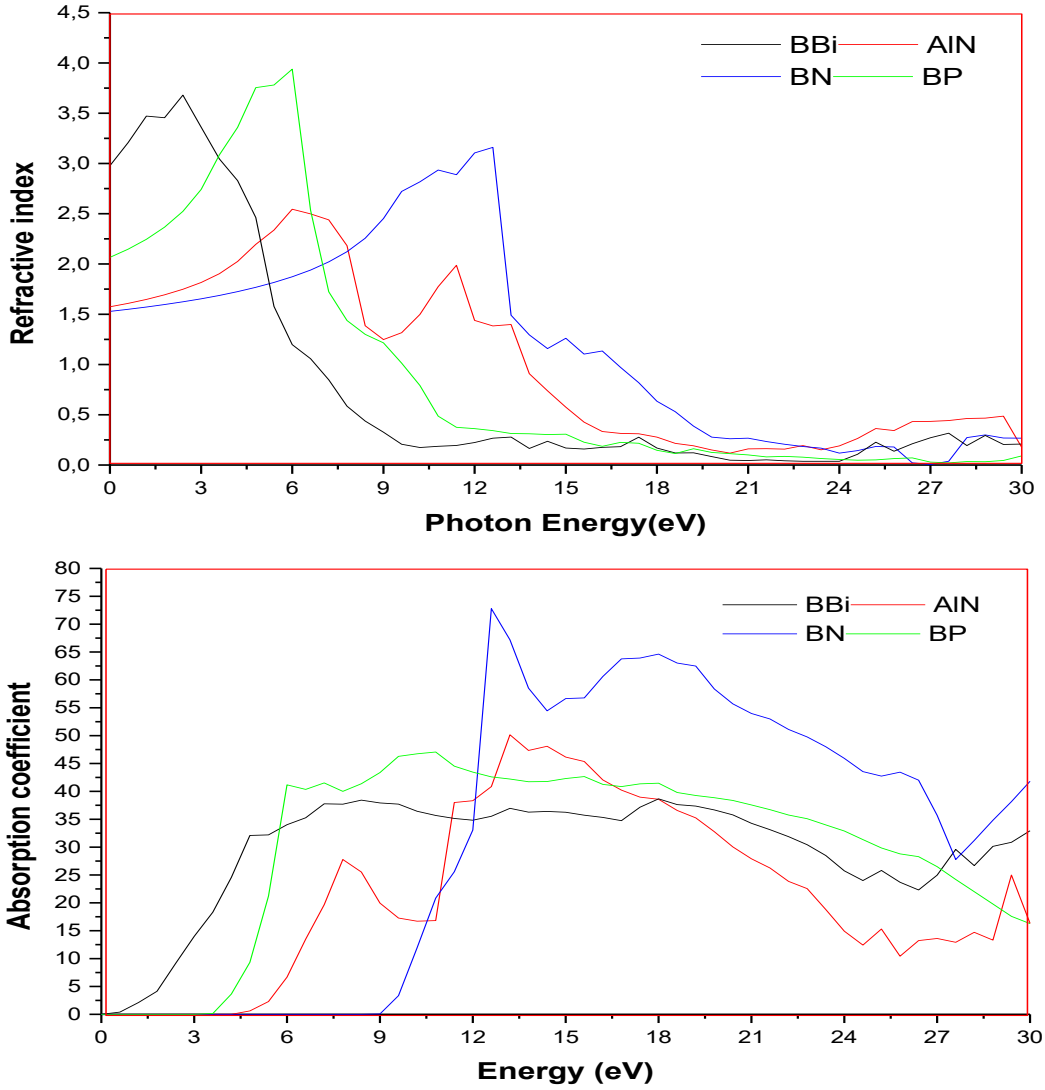

Fig. 12. Calculated refractive indices n(ω) and absorption coefficients α(ω) for binary compounds (color online)

The curves of $\varepsilon_2(\omega)$ indicate that the threshold energy (first critical point) occurs at (0.7, 2, 2 eV) in case (001) and (0, 0, 0.9 eV) in case (111) for $(BBi)_1/(BN)_1$, $(BP)_1/(BN)_1$ and $(AlN)_1/(BN)_1$, respectively. These values correspond to the electronic transition values ($\Gamma V \rightarrow MC$) of $(BBi)_1/(BN)_1$, $(BP)_1/(BN)_1$ and ($\Gamma V \rightarrow \Gamma C$) of $(AlN)_1/(BN)_1$ orientated 001. This point represents the threshold for a direct optical transition between the highest state in the valence band and the lowest state in the conduction band, which is identified as the fundamental absorption front. Beyond these points, the curve increase rapidly for SLs with direction (001) and is almost zero for SLs with direction (111). As a general observation, all the curves for the (001)-oriented SL in Figs. 13, 14 show one main peak and Fig. 15 shows three peak sappearing in the resonance behavior. We also note that the dielectric functions of the superlattice $(BBi)_1/(BN)_1$, $(BP)_1/(BN)_1$indirection (001) are approximately the same elsewhere as BN with a different position, we also note that it is very different compared to the direction (111) that contains a significant

contribution from intraband transitions [49], which shows that SLs oriented (111) have semi-metal behavior. The imaginary part of the dielectric function reflects the absorption of the material. The maximum absorption for the three SLs is located at (4.5, 6.5, 7.5 eV) in case (001) and (8, 24, 9 eV) in case (111), respectively. For oriented to (001), most optical transitions contribute to these images that occur from the occupied orbit of atoms located at the top of the valence band to the unoccupied orbit of atoms located at the bottom of the conduction band, note that the change detected in the SL 111 tracings could be attributed to the difference between the optical transition states, thus due to the overlap of the bands and the contributions of the orbitals to the Fermi level in the densities of states.

The variation of $\varepsilon_1(\omega)$ as a function of the energy of SL is represented in Figs. 13, 14, 15. We noted that these optical spectra shown in the indicated Fig. are similar to those of their BN binaries with differences in the position and height. The limiting value of the real part of the complex dielectric function obtained at an irradiation frequency close to zero is called the static dielectric constant $\varepsilon_1(0)$. For zero dispersion (the non-existense of diffusion), the absorption is maximum. Our calculated values of $\varepsilon_1(0)$ are summarized in Table 3. The static dielectric constant $\varepsilon_1(0)$ decreases toward the orientation (111). We concluded that the orientation axis has an effect on the real parts of the dielectric functions for all superlattices. The values of $\varepsilon_1(0)$ become lower for the (111) orientation compared to the (001) orientation.

Table 3. Calculated static optical constants $\varepsilon_1(0)$ and static refractive index n(0) for SL's oriented 001 and 111

Superlattice		
Compounds	$\varepsilon_1(0)$	n(0)
BBi_1BN_1 (001)	5.304	2.230
BBi_1/BN_1 (111)	2.922	1.70968
BP1/BN1 (001)	3.922	1.98047
BP_1/BN_1 (111)	2,46008	1,40288
AIN_1BN_1 (001)	3.128	1.76879
AIN_1/BN_1 (111)	1.186	1.08916

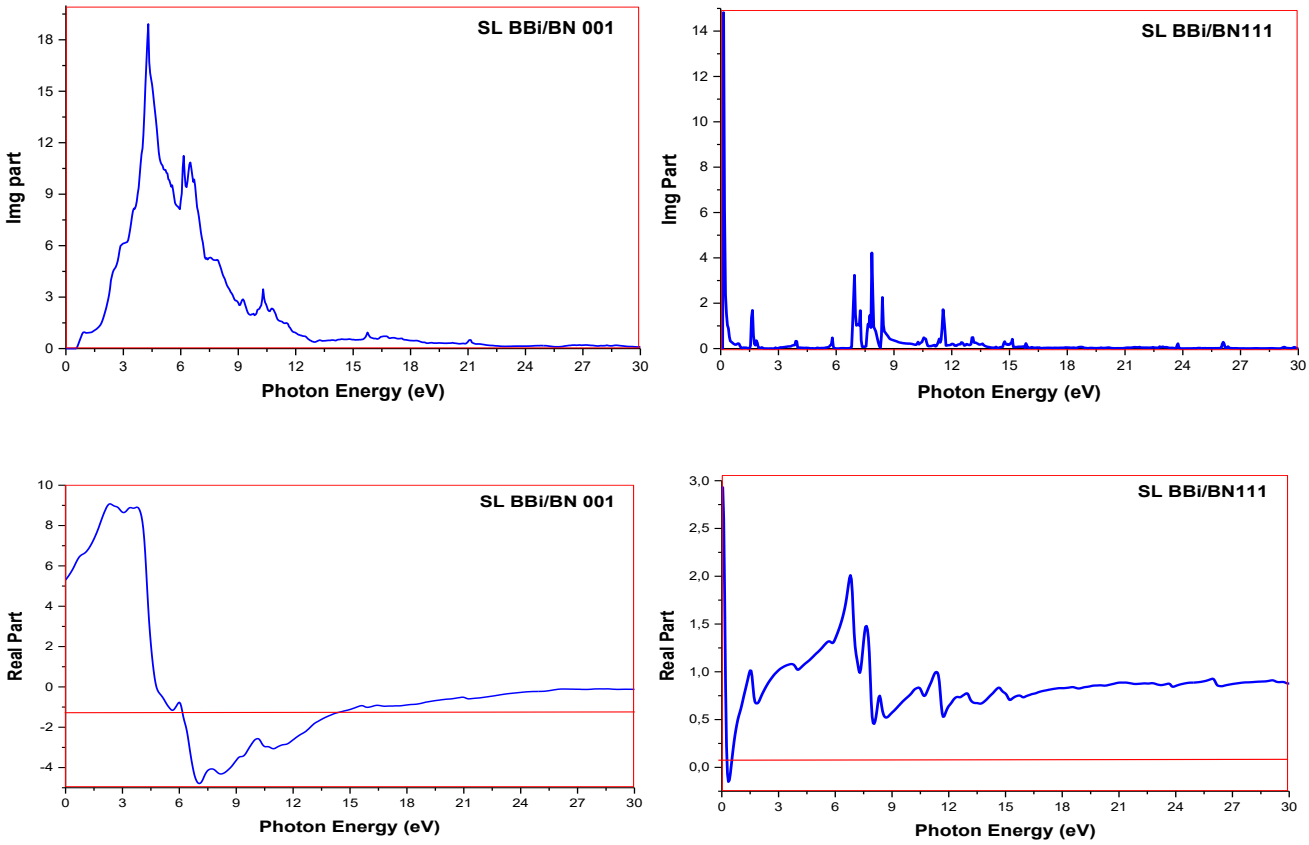

Fig. 13. Calculated dielectric functions (real and imaginary parts) for SL's$(BBi)_1/(BN)_1$ oriented (001) and (111) (color online)

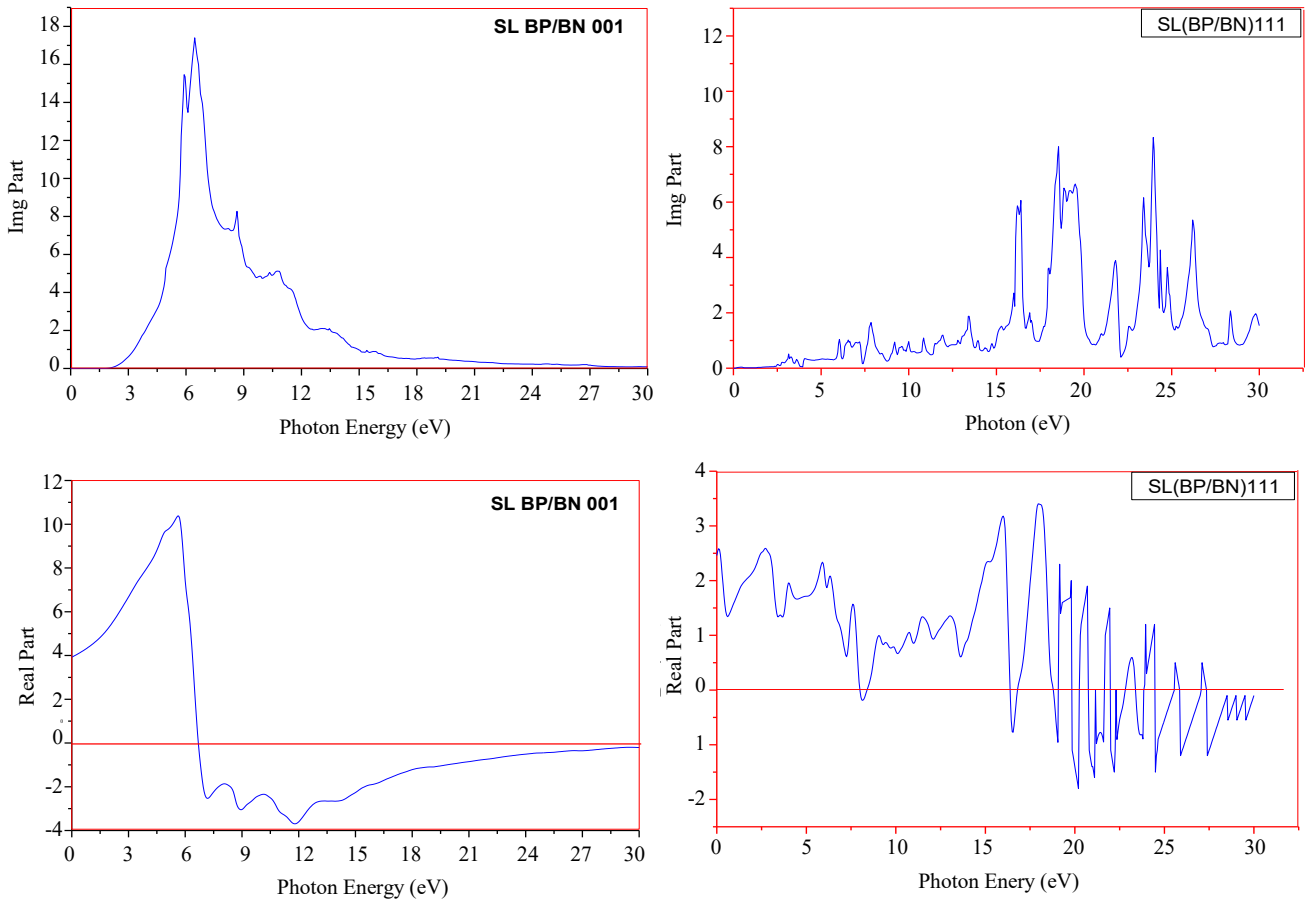

Fig. 14. Calculated dielectric functions (real and imaginary parts) for SL oriented $(BP)_1/(BN)_1$ (001) and (111) (color online)

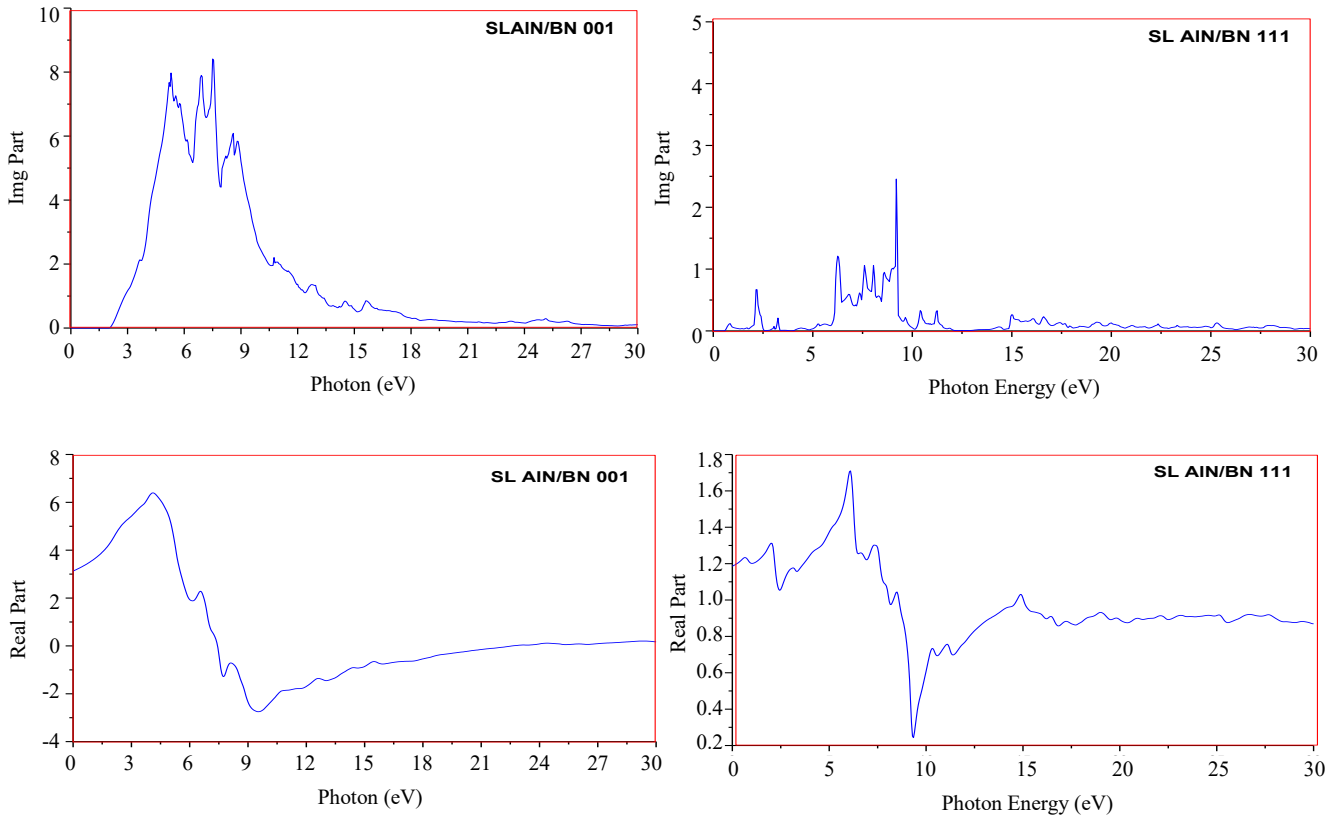

Fig. 15. Calculated dielectric functions (real and imaginary parts) for SL's $(AlN)_1/(BN)_1$ oriented (001) and (111) (color online)

The refractive index of SL's $(BBi)_1/(BN)_1$, $(BP)_1/(BN)_1$ and $(AlN)_1/(BN)_1$ is a valuable tool for the design of photovoltaic and optoelectronic devices. To study the transparency of SL in response to incident light, the relationship in Equation (7) is used to calculate the theoretical refractive index values for all SL. The refraction spectra n(x) and the static refractive index n(0) are shown in Figs. 16, 17, 18 and reported in Table 3. For the calculated SL, the static refractive indices n(0) are increased from the refraction spectra n(x). The maximum refractive index is reached for the photon energy around (4.2, 5.9, 4.54 eV) for case (001) and (0.5, 18, 5.9 eV) for case (111) of SL's $(BBi)_1/(BN)_1$, $(BP)_1/(BN)_1$,and $(AlN)_1/(BN)_1$, respectively. The refractive index spectra of the (111) SLs in Figs. 16, 17, 18 show a complete change compared to the SLs oriented (001). The primary factor that likely prevents significant changes in the optical properties of SL's 111 is the involvement of atomic orbitals in determining the Fermi level in electronic properties. To understand the optical characteristics of the SL's, calculations are performed to analyze their optical absorption spectra.

The dispersion in the optical absorption spectra of the SL in both directions is shown in Figs. 16, 17, 18. The absorption peak of SL (001) changes to a lower energy compared to its binaries and the threshold energy decreases. We observe from these curves that the absorption threshold starts from the energy values of (0.5, 2.5 and 2.25 eV) for case (001) and (0, 0, 1.5 eV) for case (111) for the SL $(BBi)_1/(BN)_1$, $(BP)_1/(BN)_1$ and $(AlN)_1/(BN)$, respectively. The SL moves towards lower energy compared to binaries. The maximum value of $\alpha(\omega)$ is around (11.3,11.2, 9 eV) for case (001) and (7.7,19,9 eV) for case (111) for the SLs $(BBi)_1/(BN)_1$, $(BP)_1/(BN)_1$ and $(AlN)_1/(BN)_1$, respectively, then the absorption coefficient decreases abruptly for the photon luminous above these energies. Calculated optical properties reveal that the title compounds are characterized by strong absorption in a large energy window including the high-energy part of the sun visible spectrum. The remarkable characteristics exhibited by superlattices oriented along the (001) direction make them highly favorable options for applications in infrared and optoelectronics.

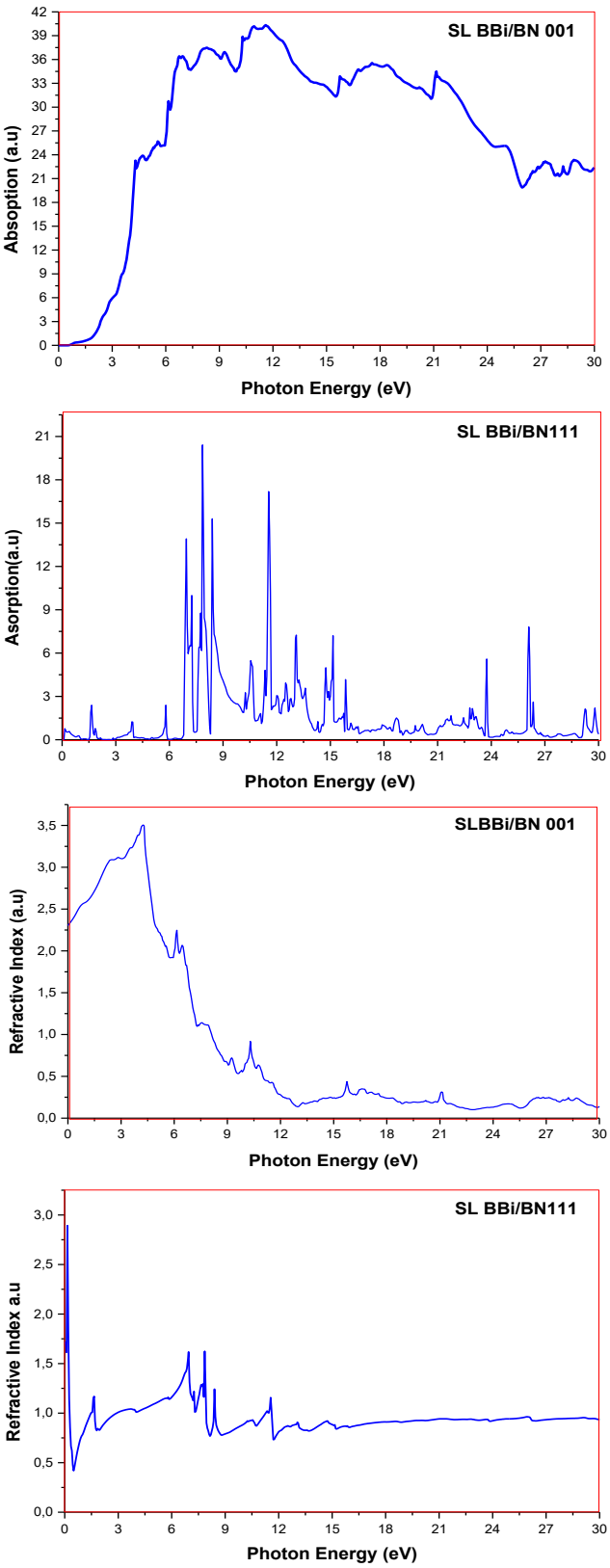

Fig. 16. Calculated refractive indices n(ω) and absorption coefficients α(ω) for SL oriented $(BBi)_1/(BN)_1$ (001) and (111) (color online)

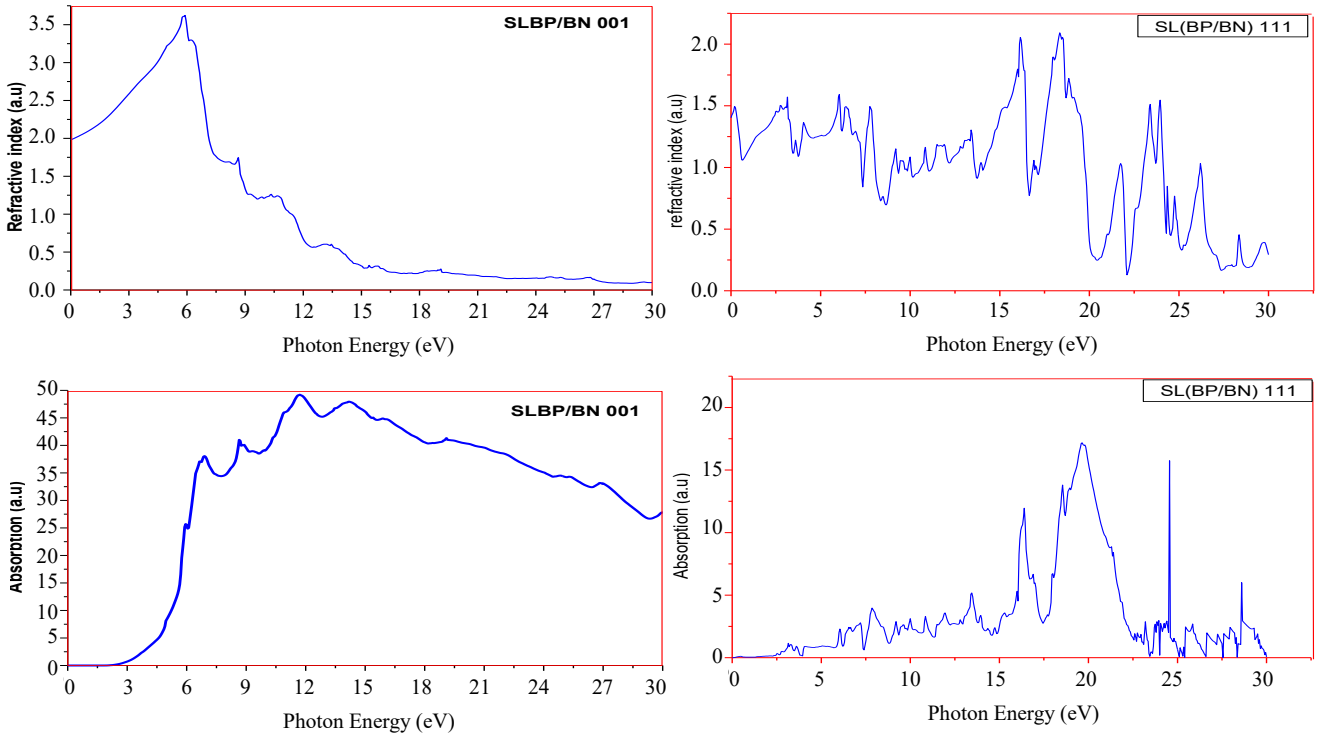

Fig. 17. Calculated refractive indices n(ω) and absorption coefficients α(ω) for SL $(BP)_1/(BN)_1$ oriented (001) and (111) (color online)

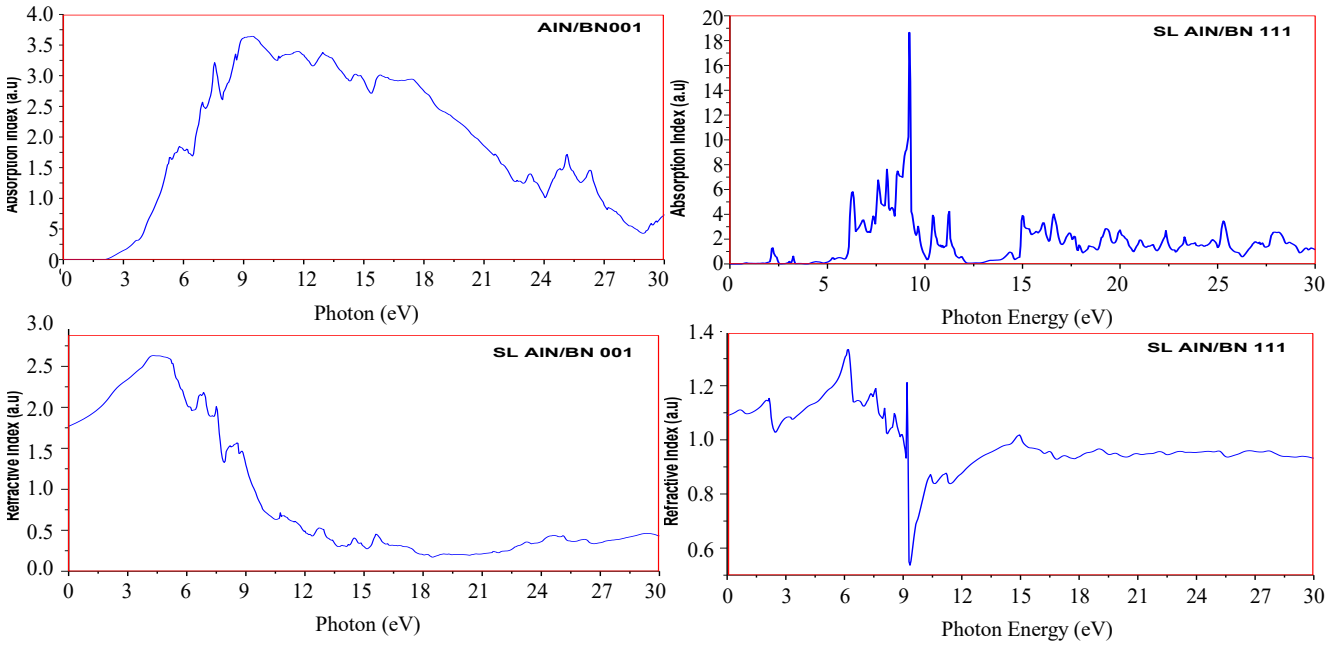

Fig. 18. Calculated refractive indices n(ω) and absorption coefficients α(ω) for the SL's $(AlN)_1/(BN)_1$ oriented (001) and (111) (color online)

4. Conclusion

Using FPLMTO+GGA96, we conducted an ab initio calculation to examine the structural, electronic and optical properties of three superlattice systems: $(BBi)_1/(BN)_1$, $(BP)_1/(BN)_1$ and $(AlN)_1/(BN)_1$. We focused on two crystal orientations, (001) and (111). Our findings reveal that the (BBi)1/(BN)1 and $(BP)_1/(BN)_1$ superlattices exhibit an indirect fundamental band gap effect, whereas the $(AlN)_1/(BN)_1$ superlattice displays a direct band gap. In terms of semiconductor behavior, the (001)-oriented superlattices demonstrate variable energy gap values, which fall within the infrared spectrum and visible emission. On the other hand, the (111)-oriented

superlattices exhibit characteristics of semimetals, with an overlap between the valence band and the conduction band. Moreover, when the charge density is calculated, it becomes evident that the behavior of BN significantly impacts the properties of the SL's. Notably, there is a subtle distinction in the contribution of atomic orbitals to the electronic properties for all (001) oriented SL's. Conversely, for (111) oriented SL's, the participation of atomic orbitals at the Fermi level becomes apparent. The dielectric functions, refractive index, and calculated absorption spectra of SL (001) indicate that these systems hold great promise for various technological applications. For (111) oriented SL's, a semimetallic behaviour is expected. The super lattices oriented along the (001) direction display remarkable properties that make them very attractive choices for optoelectronic and infrared applications.as a perspective of our work other optical properties such as transmittance, absorbance and resistivity could be addressed. There are no experimental and theoretical studies for the properties of SL oriented to (111) of $(BBi)_1/(BN)_1$, $(BP)_1/(BN)_1$ and $(AlN)_1/(BN)_1$, we hope that these results will serve as references for future studies.

Acknowledgements

The authors thank S. Y. Savrasov for the freelyav available Mindlab software. This work was supported by the Applied Materials Laboratory (A.M.L).

References

[1] Salah Daoud, Noudjoud Lebga, International Journal of Physical Research **4**(1), 1 (2016).
[2] Cihan Kürkçü, Çagatay Yamçıçıer, Solid State Communications **303–304**, 113740 (2019).
[3] M. Ustundag, M. Aslan, Battal G. Yalcin, Computational Materials Science **81**, 471 (2014).
[4] L. I. Karaouzène, A. E. Merad, T. Ouahrani, M. R. Boufatah, Optik **168**, 287 (2018).
[5] N. Mehnane, N. Oukli, M. Oukli, Chin. J. Phys. **55**, 1275 (2017).
[6] H. Kim, T. G. Andersson, J. M. Chauveau, A. Trampert, Solid State Electron. **47**, 539 (2003).
[7] Mimouna Oukli, Noureddine Mehnane, Nabila Oukli, Bachir Bachir Bouiadjra, Hafida Belghoul, Physica E: Low-dimensional Systems and Nanostructures **114**, 113653 (2019).
[8] M. Merabet, D. Rached, R. Khenata, S. Benalia, B. Abidri, N. Bettahar, S. Bin Omran, Physica B **406**, 3247 (2011).
[9] Alleg Abdelakader, Benamara Ahmed, Moulay Noureddine, Berrahal Mokhtar, Zoukel Abdelhalim, Mansour Omar, Bensaid Djillali, Azzaz Yahia, Y. Al-Douri, Solid State Communications **380**, 115435 (2024).
[10] Djamel Allali, Bouhemadou Abdelmadjid, Saad Essaoud Saber, Deghfel Bahri, Fares Zerarga, Rabie Amari, Missoum Radjai, Saad Bin Omran, Khenata Rabah, Yarub Al-Douri, Computational Condensed Matter **38**, e00876 (2024).
[11] Hatem Allaf, Missoum Radjai, Djamel Allali, Abdelmadjid Bouhemadou, Saber Saad Essaoud, Saad Bin Omran, Rabah Khenata, Yarub Al-Douri, Computational Condensed Matter **37**, e00850 (2023).
[12] Djamel Allali, Rabie Amari, Abdelmadjid Bouhemadou, Ammar Boukhari, Bahri Deghfel, Saber Saad Essaoud, Saad Bin-Omran, Missoum Radjai, Rabah Khenata, Yarub Al-Douri, Physica Scripta **98**, 115905 (2023).
[13] Jibril I. Al-Hawarin, Abdel-Aziz Abu-Yamin, Abd Al-Aziz A. Abu-Saleh, Ibrahim A. M. Saraireh, Mansour H. Almatarneh, Mahmood Hasan, Omar M. Atrooz, Y. Al-Douri, Materials **16**(14), 5160 (2023).
[14] Rachedi Samia, Azzaz Yahia, Benamara Ahmed, Berrahal Mokhtar, Moulay Noureddine, Liani Mohamed, Bensaid Djillai, Y. Al-Douri, Chemical Physics **573**, 111998 (2023).
[15] Jimmy-Xuan Shen, Darshana Wickramaratne, Chris G. Van de Walle, Physical Review Materials **1**, 065001 (2017).
[16] K. Bencherif, A. Yakoubi, H. Mebtouche, Acta Physica Polonica A **131**(1), 209 (2017).
[17] O. Arbouche, B. Belgoumène, B. Soudini, Y. Azzaz, H. Bendaoud, K. Amara, Computational Materials Science **47**, 685 (2010).
[18] A. Zaoui, D. Madouri, M. Ferhat, Philosophical Magazine Letters **89**(12), 807 (2009).
[19] Feriel Ouarda Gaid, Fatima Zohra Boufadi, Y. Al-Douri, Emergent Materials **5**, 1065 (2022).
[20] S. Y. Savrasov, Phys. Rev. B **54**, 16470 (1996).
[21] J. P. Perdew, S. Burke, M. Ernzerhof, Phys. Rev. Lett. **77**, 3865 (1996).
[22] A. Benamara, N. Moulay, Y. Azzaz, M. Ameri, M. Rabah, Y. Al-Douri, A. Bouhemadou, Ch. Moumen, Materials Today Communications **35**, 105545 (2023).
[23] Saim, F. Belkharroubi, F. Z. Boufadi, I. Ameri, L. F. Blaha, A. Tebboune, M. N. Belkaid, W. Belkilali, M. Ameri, Y. Al-Douri, A. F. Abd El-Rehim, Journal of Electronic Materials **51**, 4014(2022).
[24] Laroussi Samia, Fadila Belkharroubi, Ameri Ibrahim, Blaha Farah Lamia, Asma Saim, Ahmed Maizia, Ameri Mohammed, Y. Al-Douri, Emergent Mater. **5**, 537 (2022).
[25] M. Merabet, S. Benalia, L. Djoudi, O. Cheref, N. Bettahar, D. Rached, R. Belacel, Chinese Journal of Physics **60**, 462 (2019).
[26] Huaqing Huang, Jianpeng Liu, Wenhui Duan, Physical Review B **90**, 195105 (2014).
[27] Sadik Bagc, Battal G. Yalcin, J. Phys. D: Appl. Phys. **48**, 475304 (2015).
[28] M. Ferhat, A. Zaoui, Phys. Rev. B **73**, 115107 (2006).
[29] Battal G. Yalcin, Appl. Phys. A **122**, 456 (2016).
[30] M. Guemou, N. A. Abdiche, R. Riane, R. Khenata,

Physica B: Condensed Matter **436**, 33 (2014).
[31] M. B. Kanoun, A. E. Merad, J. Cibert, H. Aourag, Solid State Electronics **48**, 1601 (2004).
[32] A. Trampert, O. Brandt, Semiconductors and Semimetals **50**, Eds: J. L. Pankove, T. D. Moustakas, Academic Press, San Diego, p. 167 (1998).
[33] E. Knittle, R. M. Wenzcovitch, R. Jeansloz, M. L. Cohen, Nature **337**, 349 (1989).
[34] F. D. Murnaghan, Proc. Natl. Acad. Sci. U.S.A. **30**, 5390 (1944).
[35] Bachir Bachir Bouiadjra, Noureddine Mehnane, Nabila Oukli, Revista Mexicana de Fısica **67**(1), 7 (2021).
[36] Rabah Riane, Zouaoui Boussahla, Samir F. Matar, Ali Zaoui, Z. Naturforsch. **63b**, 1069 (2008).
[37] A. Zaoui, F. El Haj Hassan, J. Phys. Condens. Matter **13**, 253 (2001).
[38] Tab Slimane, «Doctoral Thesis: Etude des premiers principes des propriétés d'alliages $BBi_{1-x}N_X$»2021, Dr. Tahar Moulay University, SAIDA, Algeria.
[39] P. Blaha, K. Schwarz, P. Sorantin, S. B. Trickey, Comput. Phys. Commun. **59**, 399 (1990).
[40] A. Said, M. Debbichi, M. Said, Optik **127**, 9212 (2016).
[41] Y. Al-Douri, B. Merabet, H. Abid, R. Khenata, Superlattices and Microstructures **51**, 404 (2012).
[42] S. Alnujaim, A. Bouhemadou, M. Chegaar, A. Guechi, S. Bin-Omran, R. Khenata, Y. Al-Douri, W. Yang, H. Lu, The European Physical Journal B **95**, 114 (2022).
[43] Hela Ferjani, Youssef Ben Smida, Yarub Al-Douri, Inorganics **10**, 155 (2022).
[44] A. Laref, A. Altujar, S. Laref, S. J. Luo, Solar Energy **142**, 231 (2017).
[45] B. Tahir, A. Bouhemadou, S. Bin-Omran, R. Khenata, Y. Al-Douri, N. Guechi, Computational Condensed Matter **35**, e00809 (2023).
[46] R. M. Wentzcovitch, K. J. Chang, M. L. Cohen, Phys. Rev. B **34**, 1071 (1986).
[47] H. Meradji, S. Labidi, S. Ghemid, S. Drablia, B. Bouhafs, Physics Procedia **2**, 933 (2009).
[48] Lamia Drici, Fadila Belkharroubi, Y. Al-Douri, Emergent Materials **5**, 1039 (2022).
[49] M. Merabet, S. Benalia, L. Djoudi, O. Cheref, N. Bettahar, D. Rached, R. Belacel, Chinese Journal of Physics **60**, 462 (2019).
[50] Claudia Ambrosch-Draxl, Jorge O. Sofo, Computer Physics Communications **175**, 1 (2006).
[51] D. Allali, A. Bouhemadou, E. Muhammad Abud Al Safi, S. Bin-Omran, M. Chegaar, R. Khenata, A. H. Reshak, Physica B: Condensed Matter **443**, 24 (2014).
[52] D. P. Rai, Sandeep, A. Shankar, Anup Pradhan Sakhya, T. P. Sinha, P. Grima-Gallardo, H. Cabrera, R. Khenata, Madhav Prasad Ghimire, J. R. K. Thapa, Journal of Alloys and Compounds **699**, 1003 (2017).
[53] David R. Penn, Physical Review **128**(5), 1 (1962).
[54] B. Tahir, A. Bouhemadou, S. Bin-Omran, R. Khenata, Y. Al-Douri, N. Guechi, Computational Condensed Matter **32**, e00705 (2022).

*Corresponding author: ouklimouna22@gmail.com